Scattering-angle resolved product rotational alignment for the reaction of Cl with vibrationally excited methane

A. J. Orr-Ewing,[a] W. R. Simpson,[b] T. P. Rakitzis, S. A. Kandel, and R. N. Zare
Department of Chemistry, Stanford University, Stanford, California 94305

(Received 23 September 1996; accepted 7 January 1997)

We have applied the experimental technique of core extraction [W. R. Simpson *et al.*, J. Chem. Phys. **103**, 7299 (1995)] combined with resonance-enhanced multiphoton ionization (REMPI) with a polarized laser beam to probe the angular-momentum alignment of the HCl product of the reaction of Cl with vibrationally excited $CH_4(\nu_3=1)$. The core extraction method permits us to distinguish products scattered in different directions in the center-of-mass frame, and thus we are able to determine the rotational alignment for various product scattering angles for individual $HCl(v',J')$ quantum states (a state-resolved three-vector correlation). For the forward-scattered $HCl(v'=1,\ J'=1)$ we observe a large positive rotational alignment. This positive velocity-angular-momentum correlation is interpreted to be the result of the angular momentum of the HCl product being directed in the plane perpendicular to the line-of-centers force in a simple hard-sphere scattering model. © *1997 American Institute of Physics.* [S0021-9606(97)01114-8]

I. INTRODUCTION

Recent experiments in our laboratory[1–5] probed the differential cross section (DCS) for the reaction of Cl with CH_4 for different asymptotic vibrational and rotational quantum states of the reagent CH_4 and the product HCl. For the different state-to-state channels studied we observed striking changes in the angular scatter of the HCl. The proposed mechanism involves impact-parameter-dependent scattering with a peripheral mechanism giving rise to the forward-scattered HCl products. We tested the proposed mechanism for the observed scattering behavior by using a polarized, infrared (IR) laser beam to prepare the CH_4 and its isotopomer, CD_3H, vibrationally excited with a spatial alignment of the C–H vibrational coordinate (which we term ''vibrational alignment''). For CD_3H, this vibrational alignment corresponds to pointing the C–H bond either preferentially parallel or preferentially perpendicular to the direction of approach of the Cl atom. We demonstrated a significant steric effect, with reaction to form forward-scattered HCl enhanced by a perpendicular axis alignment. The axis-alignment effect was distinguished from rotational alignment[6] of the CH_4 or CD_3H, which also arises from the polarized IR excitation, by pumping the reagent to an excited state via different rovibrational transitions within the *P*, *Q*, and *R* branches.

The reaction $Cl+CH_4(\nu_3=1,\ J)\rightarrow HCl(v',J')+CH_3$ generates forward-, backward-, and sideways scattered HCl products. The forward-scattered component is predominant for $v'=1$, $J'=0$, 1, and 2, whereas the $v'=1$, $J'=3$ product has a backward-scattered component of comparable intensity to the forward-scattered part of the differential cross section. Product HCl formed in $v'=0$ is mostly backward and sideways scattered.[1–3] In the work presented in this paper, we used a polarized *probe* laser to measure the rotational alignment of the $HCl(v',J')$ products. The technique of core extraction[2] of the HCl^+ ions formed by resonance-enhanced multiphoton ionization (REMPI) of the nascent HCl products allows us to distinguish this rotational alignment for the forward-, sideways, and backward-scattered products. We therefore demonstrate the feasibility of studying state-to-state bimolecular reactions for which one of the *reagents* can be prepared rotationally and vibrationally aligned, and for which the dependence of the rotational alignment of one *product* on the reactive-scattering angle is determined. In the language of vector properties of reactions, such a measurement would be described as a four-vector correlation because it encompasses the relative velocity and rotational angular-momentum vectors of both the reagents and products.

To study the reaction of Cl atoms with methane, we use a photoinitiated reaction scheme in which fast chlorine atoms are produced almost exclusively (>98%) in their ground electronic state, $^2P_{3/2}$.[7] We discussed previously how a measure of the product speed distribution for a photoinitiated state-to-state reaction permits a determination of the differential cross section[8] for photoinitiated reactions, and similar results were presented by Aoiz *et al.*[9] Two strategies have developed for measuring the product speed distribution: One uses narrow bandwidth probe lasers to record product Doppler line profiles by laser induced fluorescence (LIF);[9,10] the other involves REMPI detection combined with time-of-flight (TOF) mass spectrometry to make measurements of the product velocity that reflect directly the form of the DCS.[2,3,11,12]

In addition to determining differential cross sections for bimolecular reactions, photoinitiated reaction studies are (as mentioned above) also sensitive to the correlation between product velocities (or scattering angles) and rotational angular momenta. Aoiz *et al.*[9] have considered the analysis of Doppler profiles to extract details of the velocity-angular momentum vector ($\mathbf{v}-\mathbf{J}$) correlations within the bipolar-

[a]Current address: School of Chemistry, University of Bristol, Bristol BS8 1TS, United Kingdom.
[b]Current address: Geophysical Institute, University of Alaska at Fairbanks, 903 N. Koyukuk Dr., Fairbanks, Alaska 99775-7320.

moment formalism developed by Dixon[13] for photodissociation products, and discuss the inversion of Doppler profiles via a Fourier transform (FT) method to obtain these bipolar moments. Illustrations of the FT approach include studies of the reactions of $O(^1D)$ with N_2O,[14] and CH_4.[15] Instead of the FT method, Hall and co-workers[10] fitted experimental Doppler profiles of OH formed by reaction of H with O_2 with a basis set of functions constructed for different scattering angles and rotational alignments. Recently, Brouard and co-workers[16,17] have adopted a similar basis-set analysis method; in this most recent study, Brouard *et al.* have obtained extremely detailed information for the $H+CO_2$ reaction by measuring several polarization-dependent differential cross sections for state-resolved OH products. Costen *et al.*[18] independently applied the bipolar-moment formalism of Dixon[13] to the reaction of $O(^3P)+CS$ and observed a strong preference for the CO product to rotate in a wheel-like fashion with its rotational angular momentum perpendicular to its velocity. Related work on inelastic scattering by McCaffery and co-workers[19] uses a purely spectroscopic method to study state-to-state differential cross sections and $\mathbf{v}-\mathbf{J}$ correlations for the inelastic scattering of $Li_2(A\ ^1\Sigma_u^+)$ from Xe. Their experimental strategy employs velocity selection of the $Li_2(A\ ^1\Sigma_u^+)$ by sub-Doppler laser excitation from the ground state, rather than using photodissociation to form fast atoms.

The detection of reaction products by REMPI/TOF allows velocity resolution in higher dimensions than the one-dimensional projections of Doppler profile experiments. Shafer *et al.*[11] reported the use of a three-color REMPI scheme that is Doppler selective in two dimensions (X and Y) and resolves the speed distribution along the remaining axis (Z) by time-of-flight in a linear mass spectrometer (MS). Simpson *et al.*[2,3] utilized a small aperture in a TOF/MS as a means of limiting detection to those ionized products with little or no component of velocity away from the Z axis. Valentini and co-workers[20] recently suggested an alternative scheme for three-dimensional resolution of velocity distributions of photofragments and reaction products. For a photoinitiated reaction $A+BC\rightarrow AB+C$, with C formed in one state only, a three-dimensionally resolved experiment, for which only products with $v_X=v_Y=0$ are detected, will give a data set in which each point corresponds to a different scattering angle in the center-of-mass frame. An analysis of the variation of the form and intensity of the data set (e.g., TOF profiles) with probe-laser polarization permits scattering-angle-resolved alignment parameters to be deduced.[6]

Rather than use the bipolar-moment analysis adopted by Brouard and co-workers,[9] Shafer-Ray *et al.*[21] took a different approach to determining the correlated product velocity and angular-momentum distributions. The method expresses the full spatial and angular-momentum vector distribution in terms of polarization moments of the differential cross section through straightforward formulas. The combination of velocity resolution in (almost) three dimensions with polarized-laser probing via REMPI yields these polarization moments both in the laboratory and scattering frames.

In this paper, we apply the analysis of Shafer-Ray *et al.*[21] to the reaction of $CH_4(\nu_3=1)$ with $Cl(^2P_{3/2})$ to determine the product HCl rotational alignment. In Sec. II we describe briefly the experimental apparatus employed in our study, and in Sec. III the experimental results are presented. The analysis of the data is discussed in detail in Sec. IV, and in Sec. V we then address the implications of our measurements on our understanding of the detailed dynamics of this reaction. In Appendix A we distinguish the different frames of reference for a photoinitiated reaction and the necessary formulae for extraction of polarization moments are summarized in Appendices B and C.

II. EXPERIMENT

The experimental apparatus used in this study is shown in Fig. 1 and has been described in detail elsewhere.[2,3] In brief, we injected a mixture of Cl_2 and CH_4 seeded in helium through a pulsed nozzle into the extraction region of a Wiley–McLaren configuration TOF/MS.[22] Reaction was initiated by pulsed-laser photolysis of Cl_2 at 355 nm by a frequency-tripled Nd:YAG laser (Quantel YG-581, 20 Hz). The tunable infrared output of a homebuilt $LiNbO_3$ optical parametric oscillator (OPO) pumped by the fundamental of a Nd:YAG laser (Spectra-Physics DCR-1, 10 Hz) excited CH_4 via selected rovibrational transitions to the $\nu_3=1$ state and was timed to coincide with the photolysis laser pulse. After a delay of 100–200 ns, product HCl was probed quantum state specifically by UV radiation in the region of 240 nm. This UV radiation was generated by frequency doubling in β-barium borate (BBO) the fundamental of a dye laser (Spectra Physics PDL-3) pumped by the 355-nm output of a Nd:YAG laser (Spectra-Physics DCR-2AG, 20 Hz). The dye laser operated on LD489 dye (Exciton). The probe-laser beam was linearly polarized, and a photoelastic modulator (Hinds, PEM-80) placed in the beam path allowed polarization rotation through 90° on a shot-to-shot basis. The probe laser was focused into the reaction chamber by a 500-mm focal-length quartz lens and ionized HCl via a (2+1) REMPI process. Ions were extracted into a 360-mm-long TOF tube and those that passed a small aperture (the core extractor) mounted at the end of the tube were detected by a pair of chevron-configuration microchannel plates (Galileo). The output signal from the microchannel-plate assembly was passed to a digital oscilloscope (Hewlett-Packard HP 54542A, 1 or 2 GSa/s sampling rate). Data sets were accumulated on a personal computer connected to the oscilloscope by a GPIB interface.

III. RESULTS

Experimental core-extraction TOF profiles are shown in Fig. 2 for the $HCl(v'=1,\ J'=1)$ products of the reaction $Cl+CH_4(\nu_3=1,\ J)\rightarrow HCl(v',J')+CH_3$. The products were probed on R-branch transitions of the $F\ ^1\Delta_2$-$X\ ^1\Sigma^+$ (1,1) and (0,0) bands. Profiles were recorded for two different probe-laser polarizations, parallel and perpendicular to the TOF axis. If we label the angle between the probe-laser polarization and the TOF axis as θ_d, the profiles for the different polarizations are denoted by $I_\parallel(t)$ and $I_\perp(t)$ correspond-

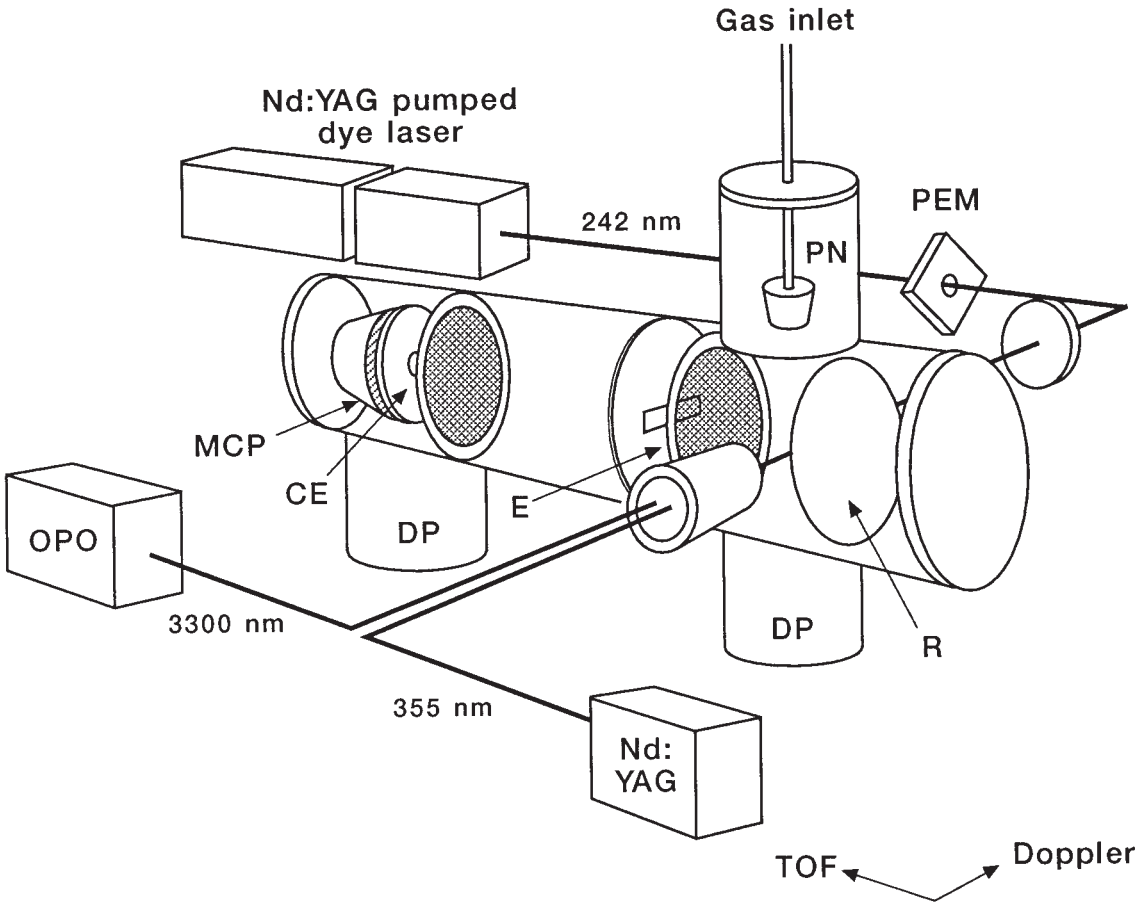

FIG. 1. Schematic diagram of the experimental apparatus. Abbreviations used in the figure are: MCP, microchannel plate; E, extractor plate; R, repeller plate; PN, pulsed nozzle; DP, diffusion pump; PEM, photoelastic modulator; OPO, optical parameteric oscillator; and CE, core extractor.

ing, respectively, to $\theta_d=0°$ and $\theta_d=90°$. The profiles shown are composites as described in the next section: The sum profile is $I_{\parallel}(t)+2I_{\perp}(t)$, and the difference profile is $I_{\parallel}(t)-I_{\perp}(t)$. The solid lines in the figure are fits to the data performed as described in Sec. IV. The general shape of each side of the sum profile reflects the form of the reactive DCS,[2,3] with the near-symmetric, double-peaked form coming from products reaching the detector that have nascent velocities either parallel or antiparallel to the TOF axis. Analysis of such profiles to obtain the DCS has been discussed in detail elsewhere.[2,3] Structure present in the difference-profile intensity for HCl($v'=1$, $J'=1$) is a consequence of product HCl rotational angular momentum alignment. Extraction of the alignment moments from these profiles is discussed in the following section. In addition to the profiles shown in Fig. 2, probe-laser polarization-dependent data were accumulated for HCl($v'=0$, $J'=3$, 5, 6, 7 and 8) and HCl($v'=1$, $J'=3$) using R-branch members of the $F\ ^1\Delta_2-X\ ^1\Sigma^+$ (1,1) and (0,0) bands. The HCl($v'=1$, $J'=3$) data showed effects consistent with the HCl($v'=1$, $J'=1$) data. For the HCl($v'=0$, $J'=3$, 5, 6, 7, and 8) data sets, the difference signals showed no discernible structure above the experimental noise levels. However, only alignment effects greater than half-maximal would be apparent with these noise levels.

IV. DATA ANALYSIS

In this section we describe the procedures used to extract scattering-angle-resolved alignment parameters from the experimental data of the preceding section. We first discuss how the REMPI signal depends on the HCl rotational alignment and the probe-laser beam polarization. We then explain how we fit the experimental data to a basis set of functions to extract alignment moments. Finally in this section, we correct the measured alignment parameters for the effects of hyperfine depolarization by the nuclear spins of the H and Cl atoms to obtain nascent alignment parameters.

A. Extraction of alignment parameters

For the purpose of alignment measurements, we probe HCl(v', J') via the $F\ ^1\Delta_2$-$X\ ^1\Sigma^+$(1,1) or (0,0) bands using (2+1) REMPI. We relate the line intensities in the REMPI spectra to the alignment moments using the general expression of Kummel *et al.*[23]

$$I=C(\det)\sum_{k,q} P_q^{(k)}(J_i,\Lambda_i,J_e,\Lambda_e,J_f,\Lambda_f,\Omega_d)A_q^{(k)}(J_i), \tag{1}$$

where the line-strength moments $P_q^{(k)}(J_i,\Lambda_i,J_e,\Lambda_e,J_f,\Lambda_f,\Omega_d)$ depend on the rotational angular momenta (J) and elec-

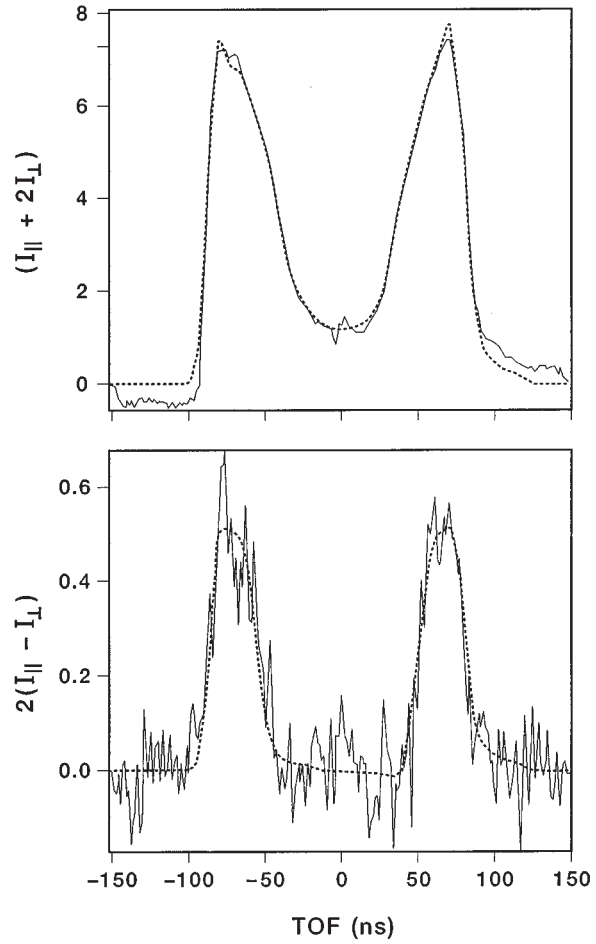

FIG. 2. Core-extraction TOF profiles obtained for HCl($v'=1$, $J'=1$) probed on the $R(1)$ line of the $F\ ^1\Delta_2$-$X\ ^1\Sigma^+$ (1,1) band by (2+1) REMPI. The two data sets shown are composites constructed from two probe laser polarizations, the isotropic sum $I_{\|}(t)+2I_{\perp}(t)$ and the anisotropic signal $I_{\|}(t)-I_{\perp}(t)$. The dashed lines through the data sets are fits to the data performed as described in the text.

tronic orbital angular momenta (Λ) of the initial (i), excited intermediate (e), and final (f) states [which, together, we henceforth abbreviate as $\{J, \Lambda\}$], as well as the experimental detection geometry (including laser polarization) which is summarized by a group of angles written here collectively as Ω_d. The constant, $C(\text{det})$, contains experimental parameters that do not vary with the polarization of the probe laser, such as the detection efficiency, the laser intensity, and the number densities of reagents and products. The $A_q^{(k)}(J_i)$ are alignment parameters describing the angular-momentum distribution in the initial state [here, HCl($v'=0$, J') or HCl($v'=1$, J')]. We use the convention that alignment refers to even moments and orientation to odd moments of the angular-momentum distribution.[6] We are insensitive to any orientation moments because we probe with a linearly polarized laser beam. Hence, the summation in Eq. (1) is limited to even values of k only. We restrict our analysis to $k=0$ and $k=2$ because we are interested exclusively in $J_i=1$ (the other data sets showing no measurable alignment effects), and for $J_i<2$, the angular-momentum distribution cannot show a hexadecapolar ($k=4$) or higher alignment moment. Our experimental procedure precludes extraction of all polarization moments because we record data at only two laser polarization angles and on a single rotational branch, but, in principle, we can determine all the alignment moments by rotating the laser polarization through a large number of angles using a half-wave plate, and detecting the product on two rotational branches. The application of Eq. (1) to the analysis of (2+1) REMPI spectra is valid provided the ionization step is saturated, so that only the two-photon absorption step, and not the ionization step, is sensitive to the angular-momentum alignment. We showed previously that we could successfully measure accurate rotational alignments of HCl under similar experimental conditions,[24] and hence the application of Eq. (1) to obtain alignment parameters from our REMPI intensities is justified.

For our simplified case, Eq. (1) reduces to the more manageable form:

$$I = C(\text{det})\{P_0^{(0)}(\{J,\Lambda\};\Omega_d)A_0^{(0)}(J_i) + P_0^{(2)}(\{J,\Lambda\};\Omega_d) \times A_0^{(2)}(J_i) + P_2^{(2)}(\{J,\Lambda\};\Omega_d)A_2^{(2)}(J_i)\}, \quad (2)$$

with alignment parameters defined in the laboratory frame (with respect to the TOF axis). The various frames of reference employed in our analysis are the same as those of Shafer-Ray *et al.*[21] and are defined in Appendix A, but the two frames of primary interest are the laboratory frame and the stationary-target frame. In the subsequent analysis we drop the explicit statement of J_i dependence of alignment parameters, but instead use labels to describe their frames of reference where appropriate.

The geometric dependencies of the $P_0^{(2)}(\{J,\Lambda\};\Omega_d)$ and $P_2^{(2)}(\{J,\Lambda\};\Omega_d)$ are very similar, with the former depending on $P_2(\cos\,\theta_d)$ and the latter on $\sin^2\,\theta_d \propto 1-P_2(\cos\,\theta_d)$, where, as stated before, θ_d is the angle between the polarization vector of the probe laser and the Z axis of the laboratory frame, and $P_2(x)=(3x^2-1)/2$ is a second Legendre polynomial.[25] Thus, without additional information, such as data recorded on a different rotational branch, it is difficult to separate the contributions from these two terms. We therefore choose to consider the likely relative contributions from the two polarization moments with $k=2$. As discussed in Appendix B, the kinematics and energetics of the reaction under study are such that the laboratory-frame moment with $k=2$ and $q=2$ is reduced by more than 90% from its stationary-target-frame value. We thus neglect this moment in our analysis and attribute all the polarization dependence of the signal to the $k=2$, $q=0$ moment. If we insert explicit forms for the line-strength moments, we obtain the simple relationship:

$$I(t;\theta_d) = \frac{I_{\text{iso}}(t)}{3}\{1 + a_{20}(t)P_2(\cos\,\theta_d)\}, \quad (3)$$

where the intensities are written as a function of time because we record time-of-flight profiles experimentally, and Eq. (3) applies to detection of a single rotational state, J_i.

$I_{iso}(t)$ is the time-of-flight profile expected for an isotropic distribution of angular-momentum vectors in the state J_i:

$$I_{iso}(t)=3C(\det)P_0^{(0)}(\{J,\Lambda\};\Omega_d)A_0^{(0)}(t). \tag{4}$$

The reaction-product speed distribution and hence the differential cross section are obtained from a knowledge of $I_{iso}(t)$. We identify $A_0^{(0)}(t)$ as being proportional to the DCS. The definitions of Eqs. (2) and (3) are related by:

$$a_{20}(t)P_2(\cos\,\theta_d)=\frac{P_0^{(2)}(\{J,\Lambda\};\Omega_d)}{P_0^{(0)}(\{J,\Lambda\};\Omega_d)}\frac{A_0^{(2)}(t)}{A_0^{(0)}(t)}. \tag{5}$$

The geometric dependence of $P_0^{(2)}(\{J,\Lambda\};\Omega_d)$ is just $P_2(\cos\theta_d)$.[23] For the case of detection of HCl on the $F\,^1\Delta_2-X\,^1\Sigma^+R(1)$ transition we make the simple identification:

$$a_{20}(t)=A_0^{(2)}(t). \tag{6}$$

The alignment parameters are written as a function of the time of flight, t, because in our experiment the time of flight is directly proportional to the nascent laboratory-frame velocity of a reaction product. As discussed in Appendix B, this velocity dependence of the laboratory-frame alignment parameters is equivalent to dependence of the alignment parameters in the scattering frame on the center-of-mass scattering angle. By writing alignment parameters as a function of time, we therefore allow for the possibility of their variation with product speed and scattering angle. The $a_{20}(t)$ are related to alignment parameters defined in the laboratory frame (and averaged over the azimuthal angle about the TOF axis) and the labeling by t is equivalent to labeling the parameters with the laboratory-frame velocity of the reaction products ($\mathbf{v}_{AB}$).

B. Data-fitting procedure

We take the laboratory-frame Z axis as being parallel to the TOF axis, and from Eq. (3) and the appropriate values of θ_d, connect the alignment parameter $a_{20}(t)$ to the polarization-dependent TOF profiles via:

$$a_{20}(t)[I_\parallel(t)+2I_\perp(t)]=2[I_\parallel(t)-I_\perp(t)]. \tag{7}$$

The linear combination of intensities, $I_\parallel(t)+2I_\perp(t)$, has no dependence on the parameter $a_{20}(t)$. If we take our experimental signals for $\theta_d=0°$ and 90° and construct the *isotropic* signal $I_{iso}(t)=I_\parallel(t)+2I_\perp(t)$, we can decompose this signal into isotropic contributions from n different center-of-mass frame scattering angles in the range $0-\pi$

$$I_{iso}(t)=\sum_{i=1}^{n} b_i I_{iso}^{(i)}(t;\theta_i), \tag{8}$$

with the ith such contributing function ($i=1,2,\ldots,n$), corresponding to a scattering angle θ_i, being

$$I_{iso}^{(i)}(t;\theta_i)=I_\parallel^{(i)}(t)+2I_\perp^{(i)}(t). \tag{9}$$

The b_i coefficients give the differential cross section. Thus, the first step in the fitting procedure is to construct a set of basis functions $I_{iso}^{(i)}(t;\theta_i)$ that assumes an isotropic distribution of angular-momentum vectors (zero alignment). The experimental data, converted to the isotropic form, $I_{iso}(t)$, is then fitted to this isotropic basis set to determine the differential cross section.

If the alignment parameter $a_{20}(t)$, referenced to the laboratory frame, for the ith scattering angle, or the ith product laboratory-frame speed, is $a_{20}^{(i)}$, then

$$a_{20}^{(i)}I_{iso}^{(i)}(t;\theta_i)=2[I_\parallel^{(i)}(t)-I_\perp^{(i)}(t)]. \tag{10}$$

Note that we drop the time dependence in the $a_{20}^{(i)}$ parameters because they correspond to a single scattering angle (or scattering-angle bin) and hence, in principle, to a single time of flight. The anisotropic (difference) signal, $A(t)$, is defined as

$$\begin{aligned}A(t)&=2[I_\parallel(t)-I_\perp(t)]\\&=2\sum_{i=1}^{n} b_i[I_\parallel^{(i)}(t)-I_\perp^{(i)}(t)],\end{aligned} \tag{11}$$

from which it follows that the anisotropic signal is given by

$$A(t)=\sum_{i=1}^{n} b_i a_{20}^{(i)}I_{iso}^{(i)}(t;\theta_i). \tag{12}$$

Thus, step two of the fitting procedure is to fit the anisotropic data sets, constructed using Eq. (11), to the isotropic basis set, $I_{iso}^{(i)}(t;\theta_i)$, and the resultant coefficients are the product of the b_i, previously determined in step one, and the alignment parameters, $a_{20}^{(i)}$. The $a_{20}^{(i)}$ can thus be determined. These alignment parameters for the different scattering angles are referred to the laboratory frame of reference, and to be dynamically useful, should be transformed into a scattering frame. The procedure for this frame transformation is discussed in Appendix B.

We find it necessary to restrict the number of basis functions used in our fitting procedure to ensure a stable and reliable fit to the anisotropy data. Thus, we restrict our angle-resolved alignment parameters to just three angular regions—forward-, sideways, and backward-scattered products. This reduction is achieved by a basis-contraction procedure built into the fitting process that collects data from 11 angular regions and further contracts the anisotropy data into three bins. We find a stable fit to the anisotropy data for four or fewer angular regions, but for a greater number of basis functions, the extracted alignment parameters fluctuate rapidly and the statistical error of the parameters is greatly increased.

C. Hyperfine depolarization

In the $X\,^1\Sigma^+$ ground electronic state of HCl, the total angular momentum, **F**, is the vector sum of the rotational angular momentum, **J**, and the total nuclear spin angular momentum of the Cl and H nuclei, **I**. For both ^{35}Cl and ^{37}Cl, the nuclear spin, $I_{Cl}=3/2$, and for the hydrogen nucleus, $I_H=1/2$. If the HCl is probed with resolution of individual J values, but without resolving the hyperfine states caused by coupling of **I** and **J**, as is the case in this work, the observed distribution of **J** will be affected by precession of **J** about **F**,

with the consequence that the rotational angular-momentum distribution is depolarized. We previously measured the hyperfine depolarization in HCl prepared rotationally aligned by IR excitation and compared the results with calculations of the expected depolarization.[24] The effect of the hyperfine depolarization is dramatic, particularly when the magnitude of **J** is comparable to the magnitude of **I**. For HCl ($v'=1$, $J'=1$) prepared at time $t=0$ with a rotational alignment parameter $A_0^{(2)}(J_i=1)=-1$, the sign of the rotational alignment parameter inverts to a positive value on a timescale of about 25 ns.[24] For the products of a reaction, formed with nascent alignment moments $A_q^{(k)}(J_i)$ over a time interval from initiation of reaction at $t=0$ to detection of reaction products at time $t=t'$, the measured alignment moments, $A_q^{(k)}(J_i;t')$ are related to the nascent alignment moments by a cumulative hyperfine-depolarization coefficient, $G_c^{(k)}(t')$:[24]

$$A_q^{(k)}(J_i;t')=G_c^{(k)}(t')A_q^{(k)}(J_i;t'=0). \tag{13}$$

Note that the time coordinate used in Eq. (13) and indicated by t' refers to the time from initiation of reaction to detection of products and therefore differs from the time coordinate of Eqs. (3)–(12) which refers to the experimental time-of-flight profile. We calculated previously the second-order ($k=2$) cumulative hyperfine-depolarization coefficients for HCl ($v=1$). We found that for $J_i=1$, the measured alignment falls rapidly from the nascent value and after about 50 ns has fallen to just 25% of that initial value, i.e., $G_c^{(k)}$ ($t'=50$ ns)$=0.25$.[24] For $J_i=5$, the measured alignment falls on a similar timescale to 75% of the nascent value. In both cases, the measured alignment then stabilizes gradually over a much longer timescale at levels slightly lower than those given above, with the further degradation a result of the additional, but slower depolarization caused by the H-atom nuclear spin. Thus, in probing the alignment of HCl($v'=1$) in low rotational states we must either limit the time between initiation of reaction (i.e., firing the photolysis and IR pump lasers) and detection of products (i.e., firing the probe laser) to intervals of less than about 40 ns, or must accept a large reduction in the measurable alignment and correct for hyperfine depolarization to determine the nascent alignment. The latter approach is the only practical solution because for a time delay between initiation and probing of only 40-ns insufficient time exists for build-up of reaction products to a detectable level. Experiments detecting $H^{35}Cl(v'=1, J'=1)$ product were conducted at a time delay of 200 ns. At this time delay, the $k=2$ cumulative hyperfine-depolarization coefficient, $G_c^{(k)}(t')=0.25$. The values and uncertainties of the $a_{20}^{(i)}$ parameters for the $H^{35}Cl(v'=1, J'=1)$ product are divided by this factor.

D. Alignment parameter values

The values of the $a_{20}^{(i)}$ parameters for all rovibrational states probed except the HCl($v'=1$, $J'=1$) are zero to within the precision of the measurements. HCl($v'=1$, $J'=1$), however, shows a substantial alignment effect. As discussed in Sec. IV B we limit our analysis to three angular regions that correspond to the ranges of scattering angle $-1\leqslant\cos\theta_r\leqslant-4/11$ (backward scatter), $-4/11<\cos\theta_r\leqslant4/11$ (sideways scatter), and $4/11<\cos\theta_r\leqslant1$ (forward scatter). These choices of angles arise because we subdivide the angular scattering up into 11 bins to fit the differential cross sections, but then reduce this angular resolution to 3 bins to give a stable fit to the alignment data. The DCS data show that the HCl($v'=1$, $J'=1$) reaction product is primarily forward scattered and thus that the alignment parameter for this angular region is most reliable. The values we obtain for $A_0^{(2)}$ (stf) after extracting the a_{20} coefficients for the three angular regions from the fit are listed in Table I. The parameters listed in Table I have been corrected for the hyperfine depolarization discussed in Sec. IV C. Note that we have omitted the time dependence of a_{20} and other alignment parameters because the parameters are averaged over three different time (or scattering angle) bins and are thus distinguished by the nature of the bin (forward, sideways or backward), as discussed in Appendix C. The alignment parameters can be related to the polarization moments of Shafer-Ray *et al.*[21] using Eq. (B2.7) or (B2.8) from Appendix B. The values of the alignment parameters for backward-scattered HCl($v'=1$, $J'=1$) must be treated with some caution in light of the fact that very little HCl($v'=1$, $J'=1$) is actually scattered into the backward hemisphere.

TABLE I. Alignment parameters for foward-, sideways, and backward-scattered HCl($v'=1,J'=1$) in the stationary-target frame. The stf values have been corrected for hyperfine depolarization effects. The confidence limits are 2σ.

HCl scattering direction	$A_0^{(2)}$ (stf)
Forward	0.28±0.07
Sideways	0.36±0.14
Backward	−0.24±0.11

As a test of the robustness and reliability of the fitting procedure, we also employed a Legendre polynomial basis set with basis functions weighted by $P_n(\cos\theta_r)$, rather than using a basis set that was constructed from functions uniformly stepped in the angular interval $\cos\theta_r$. The DCS and alignment parameters were recovered in exactly the same way as described above, and we found reliable fits to the anisotropy data for a basis set consisting of three Legendre moments. The DCS and angle-resolved alignment parameters agreed with the results of the original fitting procedure to within experimental errors.

V. DISCUSSION

In our earlier studies of the reaction of $Cl+CH_4(\nu_3=1)$ and $Cl+CD_3H(\nu_1=1)$ we demonstrated through measurements of the state-to-state DCSs and the effects of *reagent* alignment that the forward-scattered reaction product came from collisions at large impact parameters that are preferentially side-on to a C–H bond. A hard-sphere interpretation of the DCSs allowed Simpson *et al.*[4,5] to extract maps of the ranges of impact parameters leading to different reactive scattering directions. The suggestion of a peripheral reaction mechanism has been supported by QCT calculations for the

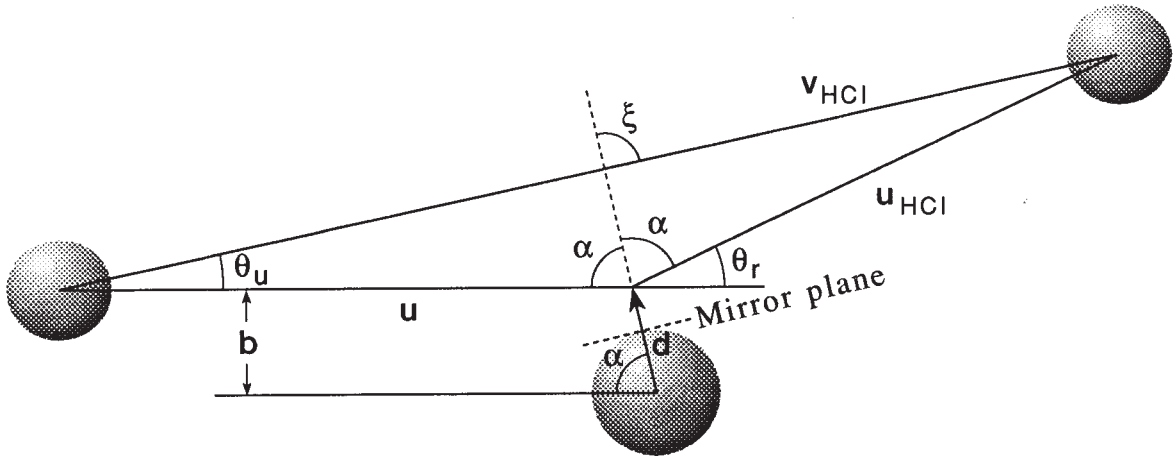

FIG. 3. Newton diagram showing the vectors and angles used in the hard-sphere scattering model interpretation of the product rotational alignment.

$Cl+CH_4$ reaction by Levine and co-workers,[26] and also by related calculations on the reaction of $Cl+HD(v=1)$ by Aoiz and Bañares.[27] It is further reinforced by recent quantum-mechanical (QM) scattering calculations by Manolopoulos and co-workers[28] for the reaction of $F+H_2$, for which the near-thermoneutral channel shows forward-scattered $HF(\nu'=3)$ as a result of reaction of high-angular-momentum partial waves. The reaction of these partial waves is enhanced by tunnelling through the centrifugal barrier.

The strong positive alignment observed for the $HCl(v'=1, J'=1)$ reaction product is close to its maximum value (including the effects of hyperfine depolarization), and is a very unusual observation. Theoretical treatments of the reaction have, to date, not made any predictions about the expected alignment. We first consider kinematic arguments to illustrate that the alignment is not a consequence of kinematic constraints and proceed to argue that the alignment is a feature of the reaction dynamics and the geometry of the reaction transition-state region.

Conservation of angular momentum requires that $\mathbf{J}+\mathbf{L}=\mathbf{J}'_{tot}+\mathbf{L}'$, where $\mathbf{L}$ and $\mathbf{L}'$ are the orbital angular momenta and $\mathbf{J}$ and $\mathbf{J}'_{tot}$ the rotational angular momenta of the reagents (unprimed symbols) and products (primed symbols) respectively. $\mathbf{J}'_{tot}$ is the sum of the HCl ($\mathbf{J}'$) and CH_3 rotational angular momenta. For reaction resulting in $HCl(v'=1, J'=1)$, the kinematics of the reaction are such that we expect $\mathbf{L}\approx\mathbf{L}'$. The magnitudes of the orbital angular momenta will be large for reaction of fast-moving reagents at the high impact parameters that lead to forward-scattered, similarly fast-moving products. The magnitudes of the rotational angular momenta of the jet-cooled reagents and rotationally cold HCl products are small. The lack of rotational excitation of the HCl implies a similarly cold rotational distribution of the CH_3 product because of the nonimpulsive transfer of a light atom during the reaction. Because $\mathbf{L}\approx\mathbf{L}'$, the relative velocities of the reagents and products ($\mathbf{u_r}$ and $\mathbf{u'_r}$, respectively) are confined to a plane perpendicular to $\mathbf{L}$ and $\mathbf{L}'$, but no such constraint exists on the reagent and product rotational angular momenta. We would anticipate impulsive transfer of the hydrogen atom within the plane of the relative velocities to induce a negative alignment because $\mathbf{J}'$ would necessarily be perpendicular to the plane of the three-atom collision. If, however, the H atom is transferred in a direction that does not lie in the plane of the relative velocities, $\mathbf{J}'$ can be aligned with a substantial component in the plane of $\mathbf{u_u}$ and $\mathbf{u'_r}$.

For the case of $Cl+CH_4(\nu_3=1)\rightarrow HCl(v'=1, J'=1)+CH_3$, we propose the following interpretation of the positive rotational alignment, which is based on the hard-sphere scattering interpretation of the differential cross sections discussed by Simpson *et al.*[5] and for which the vectors and angles defining the scattering are illustrated in Fig. 3. The transfer of H between C and Cl is known to occur via a side-on attack to give forward-scattered $HCl(v'=1, J'=1)$, whereas backward scattering of HCl arises from small-impact-parameter collisions along a C–H bond. In the hard-sphere model, the scattering angle is determined by the impact parameter according to the relationship $\cos\theta_r=2b^2/d^2-1$, where d is the distance between the hard-sphere centers at the point of impact. The main source of rotational angular-momentum alignment in our model is taken to be the relative motion of the H atom as it transfers from C to Cl. The force in a hard-sphere collision is along the line of centers of the colliding spheres. Rotation of the HCl product that is induced by this force has an angular-momentum perpendicular to, and cylindrically symmetric about, the direction of this force. We define a vector along the line of centers as $\mathbf{d}$ (with magnitude d), and, as illustrated in Fig. 3, define the angle between the $\mathbf{d}$ and $\mathbf{u}_{HCl}$ as α, so that the angle between $\mathbf{d}$ and the relative velocity of the reagents, which is parallel to $\mathbf{u}$, is π-α. The angles α and θ_r are related by $2\alpha+\theta_r=\pi$. Figure 3 also shows the laboratory-frame velocity of the reaction products, $\mathbf{v}_{HCl}$, which lies at an angle θ_u to $\mathbf{u}$ (see Appendix A). Thus, we can transform the alignment about $\mathbf{d}$ to alignment about the vectors $\mathbf{u}$, $\mathbf{u}_{HCl}$, or $\mathbf{v}_{HCl}$. Alignment in the stationary-target frame (about $\mathbf{v}_{HCl}$) is of particular relevance for interpretation of the data presented

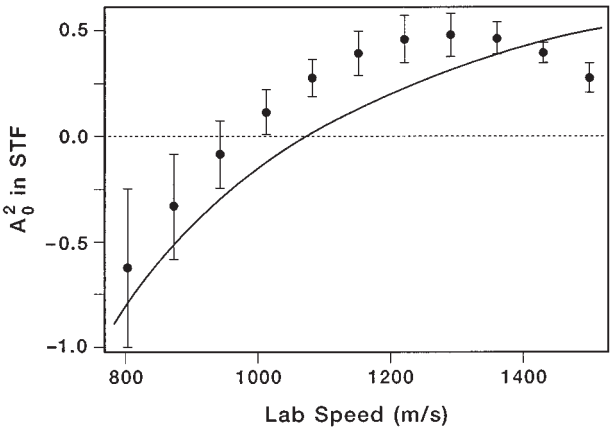

FIG. 4. Comparison of the experimental rotational alignment values in the stationary-target frame with values predicted by the model described in Sec. V and calculated using Eqs. (14) and (16). Error bars are 2σ.

here and is summarized in Table I. The angle between **d** and $\mathbf{v}_{\mathrm{HCl}}$, denoted by ξ, is given by

$$\xi = \left(\frac{\pi}{2} + \frac{\theta_r}{2} - \theta_u \right). \tag{14}$$

We can relate the rotational alignment of the HCl about the line-of-centers direction to the rotational alignment in the stationary-target frame by the frame rotation of alignment parameters from the frame of **d** to the frame of $\mathbf{v}_{\mathrm{HCl}}$

$$A_0^{(2)}(\mathrm{stf}) = \sum_q D_{q0}^{(2)}(\Omega) A_q^{(2)}(\hat{\mathbf{d}}). \tag{15}$$

The frames of reference of the alignment parameters are indicated by the terms in parentheses, and Ω denotes the Euler angles connecting the two frames of reference. Invoking cylindrical symmetry of $\mathbf{J}'$ about **d**, however, all terms in the summation with $q \neq 0$ vanish and Eq. (15) reduces to

$$A_0^{(2)}(\mathrm{stf}) = P_2(\cos\,\xi) A_0^{(2)}(\hat{\mathbf{d}}). \tag{16}$$

$P_2(\cos\,\xi)$ is evaluated using Eq. (14) and is negative for strongly forward-scattered products ($\theta_r \approx 0°$, $\alpha \approx 90°$, $\theta_u \approx 0°$) and positive for backward scattering ($\theta_r \approx 180°$, $\alpha \approx 0°$, $\theta_u \approx 0°$). The alignment parameter, $A_0^{(2)}(\hat{\mathbf{d}})$, takes the value -1 in our model because $\mathbf{J}'$ is perpendicular to **d**. Thus, the alignment in the stf is negative for backward-scattered products but becomes positive for forward scattering. Equation (16) is evaluated and plotted for all scattering angles in Fig. 4 together with the experimentally determined, scattering-angle-resolved rotational alignments of the HCl($v'=1$, $J'=1$) evaluated by fitting our data using a Legendre-polynomial basis set (see Sec. IV D). Clearly, the model describes the measured alignments very well. Despite this straightforward interpretation of the positive rotational alignment of the forward-scattered HCl($v'=1$, $J'=1$), the mechanistic origin of the propellerlike rotation of the HCl with its rotational angular momentum and velocity preferentially near parallel is not obvious. In Fig. 5, we show a schematic diagram of the type of H-atom transfer dynamics that leads

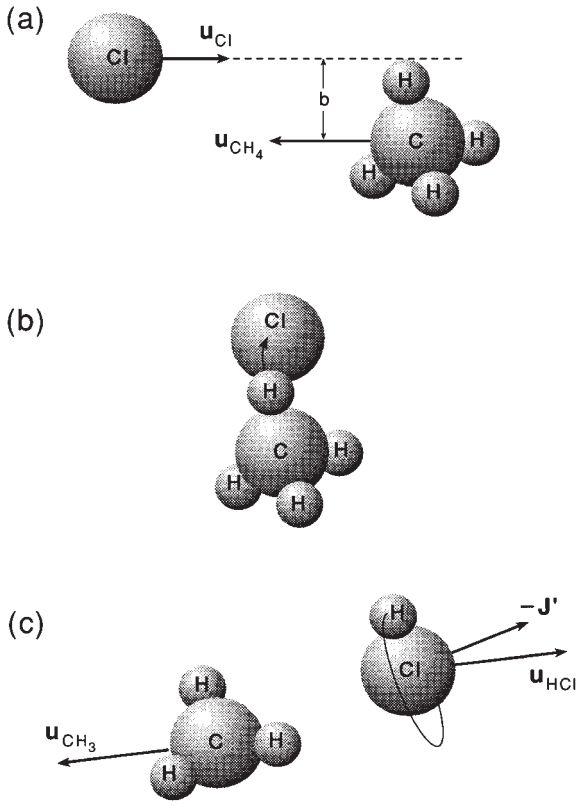

FIG. 5. Schematic diagram of the proposed mechanism for H-atom abstraction to form HCl($v'=1$, $J'=1$) with a positive correlation between the $\mathbf{J}'$ and $\mathbf{u}_{\mathrm{HCl}}$ vectors.

to a positive rotational alignment, with the key feature of the dynamics being that the H atom is transferred also *out of the plane* of the reagent and product relative velocities, as well as in the scattering plane.

The HCl($v'=1$, $J'=1$) product with a laboratory-frame speed consistent with sideways scattering shows an alignment in the stf of the same sign and similar magnitude to the forward-scattered product. As illustrated in Fig. 4, this observation is feasible for sideways scattered products. An ambiguity remains, however, because as discussed by Simpson *et al.*,[3] forward-scattered HCl($v'=1$, $J'=1$) formed in coincidence with CH_3 excited with one quantum of umbrella-mode (ν_2) vibration can result in the same laboratory speed for the HCl as sideways scattering in coincidence with $CH_3(\nu_2=0)$, and our determination of scattering angles is based on laboratory-frame speed measurements. The observed alignment in the stf is thus also consistent with the formation of forward-scattered HCl($v'=1$, $J'=1$) generated in coincidence with $CH_3(\nu_3=1)$.

VI. CONCLUSIONS

We have performed a detailed study of the rotational alignment of the HCl(v', J') products of the reaction of $Cl(^2P_{3/2})$ with $CH_4(\nu_3=1)$ to shed further light on the rich and varied dynamics of this reaction. We found that the backward-scattered HCl($v'=1$, $J'=1$) shows a preferential

negative alignment of its rotational angular-momentum vector with respect to its relative velocity (i.e., in the frame of the relative velocity vector, the population of states with $M_{J'}=0$ exceeds that of states with $M_{J'}=\pm 1$). For the forward- and sideways scattered HCl($v'=1$, $J'=1$), however, the opposite is true, and the measured *positive* rotational alignment reflects a preferential population of $M_{J'}=\pm 1$ states rather than states with $M_{J'}=0$. The variation of the alignment with scattering angle for this particular state-to-state reaction channel is successfully accounted for using a simple (hard-spherelike) model in which the product scattering angle is determined by the impact parameter for the collision, and the direction of the rotational angular-momentum vector of the product HCl is in the plane perpendicular to the line-of-centers force in the scattering process.

ACKNOWLEDGMENTS

AJOE thanks the Royal Society for the award of the Eliz. Challenor Research Fellowship. This work is supported by the National Science Foundation (NSF-CHE 9322690).

APPENDIX A: FRAMES OF REFERENCE

We adopt the frames of reference for a photoinitiated reaction studied with 3-D velocity resolution as defined by Shafer-Ray *et al.*[21] and summarize these frames here. The reagent and product scattering frames and the stationary target frame are referred to in general terms as scattering frames in the text. For a bimolecular reaction $A+BC\rightarrow AB+C$, we define $\mathbf{u}_r$ and $\mathbf{u}_r'$ as the relative velocities of reagents and products respectively, $\mathbf{u}_{AB}$ as the component of the product relative velocity for the AB product, $\mathbf{v}_{AB}$ as the laboratory-frame velocity of AB, and $\boldsymbol{\epsilon}$ as the polarization vector of the linearly polarized photolysis laser beam used to initiate reaction.

1. The reagent scattering frame (rsf)

$\hat{\mathbf{z}}^{\mathrm{rsf}}$ is taken to be parallel to the relative velocity for the reagents: $\hat{\mathbf{z}}^{\mathrm{rsf}}\|\mathbf{u}_r$. $\hat{\mathbf{y}}^{\mathrm{rsf}}$ is perpendicular to the plane of $\mathbf{u}_r$ and $\mathbf{u}_r'$.

2. The product scattering frame (psf)

$\hat{\mathbf{z}}^{\mathrm{psf}}$ is taken to be parallel to the relative velocity for the products: $\hat{\mathbf{z}}^{\mathrm{psf}}\|\mathbf{u}_r'$. $\hat{\mathbf{y}}^{\mathrm{rsf}}$ is perpendicular to the plane of $\mathbf{u}_{\mathrm{r}}$ and $\mathbf{u}_r'$.

3. The stationary-target frame (stf)

$\hat{\mathbf{z}}$ is chosen to be parallel to $\mathbf{v}_{AB}$, the lab-frame velocity of the reaction products, which is better defined experimentally than $\mathbf{u}_r$. The y axis is as defined in the reagent scattering frame. The stationary-target frame is related to the reagent scattering frame by a rotation about the y^{rsf} axis through an angle θ_u, and to the product scattering frame by rotation about y^{rsf} (or y^{psf}) through an angle θ_{AB}, where $\cos\theta_u=\hat{\mathbf{v}}_{AB}\cdot\hat{\mathbf{u}}$ and $\cos\theta_{AB}=\hat{\mathbf{v}}_{AB}\cdot\hat{\mathbf{u}}_{AB}$.

4. The laboratory frame

In an experiment we measure the correlated distribution of $\mathbf{J}$ with $\mathbf{v}_{AB}$ and $\boldsymbol{\epsilon}$. We take the laboratory frame Z axis parallel to $\mathbf{v}_{AB}$ and the Y axis perpendicular to the plane of $\boldsymbol{\epsilon}$ and $\mathbf{v}_{AB}$. $\boldsymbol{\epsilon}$ lies in the XZ plane at an angle θ_ϵ from Z. Note that the core-extraction technique ensures that $\mathbf{v}_{AB}$ is parallel to the TOF axis, and hence that the detection and laboratory frames are coincident.

The polarization moments of the differential cross section used in this paper have been referenced to the stationary-target frame, so angular momentum distributions are described in terms of the $\mathbf{v}_{AB}$ axis. It is perhaps more dynamically useful to understand how the scattering angles of the products correlate with their rotational angular momenta expressed in a frame with the z axis taken parallel to the reagent relative velocity (the scattering frame) or the product relative velocity (the product scattering frame). The interconversion between the stationary-target frame and these other reference frames is straightforward and requires a single rotation about the y axis of the stationary-target frame.

To transform from the stationary-target frame to the scattering frame, we must rotate polarization moments through an angle $-\theta_u$ about y using Wigner rotation matrices.[25] In a similar manner, the moments in the stationary-target frame can be transformed to the product scattering frame via rotation about the y axis through an angle θ_{AB} where $\cos\theta_{AB}=\hat{\mathbf{v}}_{AB}\cdot\hat{\mathbf{u}}_{AB}$. To obtain values of, for example, the second-order polarization moments in the scattering frame, we need to know the stationary-target frame values for the moments with $k=2$, and $q=0,1,2$. Note, however, that for strongly forward- or backward-scattered products, for which $\theta_u\approx 0$, $\theta_{AB}\approx 0$ or π, and $\theta_r\approx 0$ or π, the three frames coincide and moments with $q\neq 0$ vanish.

APPENDIX B: POLARIZATION MOMENTS OF THE DIFFERENTIAL CROSS SECTION

We consider a general, photoinitiated, state-to-state bimolecular reaction,

$$AX+h\nu\rightarrow A+X,$$

$$A+BC(v,J)\rightarrow AB(v',J')+C,$$

conducted under experimental conditions for which the reagent BC has no velocity; these conditions are achieved to good approximation by coexpanding BC and the precursor AX, seeded in a carrier gas such as helium, through a pulsed nozzle. The photodissociation step is performed by a linearly polarized laser and the A and X fragments recoil with an angular distribution about the laser polarization described by the anisotropy parameter β_{phot}. We assume that the AB products are probed quantum state specifically by a laser-based method such as REMPI and the velocities of the products in the laboratory frame are measured with three-dimensional resolution, i.e., we use a detection method such as core extraction.[2,3] The laser-based detection permits measurement of the polarization moments of the BC angular-momentum distribution in the laboratory frame. Shafer-Ray *et al.*[21] give

the moments of the polarization-dependent velocity distribution in the laboratory frame for a three-dimensionally resolved experiment:

$$f_{k0}^{\rm lab}(\mathbf{v}_{AB}) = \frac{1}{2uu_{AB}v_{AB}}\,[1+\beta_{\rm phot}P_2(\cos\,\theta_u)P_2(\cos\,\theta_\epsilon)] \times\left(\frac{1}{\sigma}\frac{d\sigma_{k0}}{d\Omega_r}\right), \tag{B1}$$

$$f_{k1}^{\rm lab}(\mathbf{v}_{AB}) = \frac{-3\beta_{\rm phot}\,\sin(2\theta_u)}{16uu_{AB}v_{AB}}\,[\sin(2\theta_\epsilon)]\left(\frac{1}{\sigma}\frac{d\sigma_{k1}}{d\Omega_r}\right), \tag{B2}$$

$$f_{k2}^{\rm lab}(\mathbf{v}_{AB}) = \frac{3\beta_{\rm phot}\,\sin^2\,\theta_u}{16uu_{AB}v_{AB}}\,[\sin^2\,\theta_\epsilon]\left(\frac{1}{\sigma}\frac{d\sigma_{k2}}{d\Omega_r}\right), \tag{B3}$$

$$f_{kq}^{\rm lab}(\mathbf{v}_{AB}) = 0 \quad \text{for } |q|>2, \tag{B4}$$

and

$$f_{k-q}^{\rm lab}(\mathbf{v}_{AB}) = (-1)^q f_{kq}^{\rm lab}(\mathbf{v}_{AB})^*. \tag{B5}$$

The polarization moments of the differential cross section, $(1/\sigma)(d\sigma_{kq}/d\Omega_r)$, are defined in the stationary target frame. Formal definitions of all the terms used here are stated elsewhere.[21] θ_ϵ is the angle between the electric vector of the polarized photolysis laser and the velocity vector of the detected AB products. Note that for a 3-D resolved velocity measurement, $\mathbf{v}_{AB}$ is parallel to the selected laboratory-frame axis, such as the TOF axis for a core-extraction experiment. θ_u is the angle between the relative velocity of the reagents (also the velocity of the center of mass for the collision, $\mathbf{u}$) and $\mathbf{v}_{AB}$. This angle is uniquely defined for any particular BC product speed u_{AB} in the center-of-mass frame by

$$\cos\,\theta_u = \frac{v_{AB}^2+u^2-u_{AB}^2}{2v_{AB}u}. \tag{B6}$$

Equations (B1)–(B5) demonstrate that we cannot determine moments of the angular-momentum distribution with $|q|>2$ and we limit our consideration to moments with $k\leqslant 2$ because we concentrate in this paper on HCl ($v'=1$, $J'=1$). The measurements described in this paper are restricted to values of $\theta_d=0°$ and 90°, and $\theta_\epsilon=90°$; symmetry considerations ensure that polarization moments with $q=\pm 1$ can be neglected at these laboratory-frame angles. We are thus left only with the polarization moments $f_{00}^{\rm lab}(\mathbf{v}_{AB})$, $f_{20}^{\rm lab}(\mathbf{v}_{AB})$, and $f_{22}^{\rm lab}(\mathbf{v}_{AB})$. The last of these three moments vanish if the photodissociation anisotropy parameter is zero. A knowledge of these three polarization moments tells us the more dynamically useful values of the polarization moments of the differential cross section, and clearly we are also restricted to the three values of these DCS moments with $k=0$, $q=0$, $k=2$, $q=0$, and $k=2$, $q=2$.

For the experiments described in this paper on the reaction of $Cl+CH_4(\nu_3=1)$ to form $HCl(v'=1)$ the kinematics and energetics are such that θ_u is constrained to angles between 0° and 18°. Within this range the maximum value of $\sin^2\,\theta_u$ is 0.095 and this, combined with the other multiplicative factors in Eq. (B3) means we can reasonably expect that the primary contribution to any polarization effects seen in the core extraction data will come from the $f_{20}^{\rm lab}(\mathbf{v}_{AB})$ moment and not from the $f_{22}^{\rm lab}(\mathbf{v}_{AB})$ moment.

To interpret polarization dependencies of the experimental signal, we must make the connection between the polarization moments of Eqs. (B1)–(B5) and the more familiar alignment parameters, $A_q^{(k)}$. Combining Eqs. (B1) and (29) of Shafer-Ray *et al.*,[21] we could make this connection in terms of scattering-angle averaged alignment parameters but we choose here to use *scattering-angle dependent* alignment parameters:

$$A_q^{(k)}(\theta_r) = (\delta_{k2}+1) \times\left\{\frac{(2J+1+k)!}{(2J+1)!2^k[J(J+1)]^{k/2}}\right\}{\rm Re}\left(\frac{1}{\sigma}\frac{d\sigma_{kq}}{d\,\cos\,\theta_r}\right), \tag{B7}$$

which are averaged over the azimuthal scattering angle, φ_r.

Just as we relate the regular alignment parameters to the moments of the polarization-resolved differential cross section, so we can express a relationship between the $f_{kq}^{\rm lab}(\mathbf{v}_{AB})$ and laboratory-frame alignment parameters. These laboratory-frame alignment parameters are dependent on the laboratory-frame speed of the products, v_{AB}, which has a one-to-one relationship with the center-of-mass frame scattering angle, θ_r. As above, we obtain the relationship:

$$A_q^{(k)}(v_{AB}=v_z) = (\delta_{k2}+1)\left\{\frac{(2J+1+k)!}{(2J+1)!2^k[J(J+1)]^{k/2}}\right\} \times{\rm Re}[f_{kq}^{\rm lab}(v_{AB}=v_z)], \tag{B8}$$

where we have equated the lab-frame speed of the products, v_{AB}, with the laboratory-frame speed along the Z axis because for a perfect core-extraction experiment we only detect products with velocity components $v_X=v_Y=0$, $v_Z=v_{AB}$. The connection between the speed-dependent alignment parameters in the laboratory frame, which we measure, and the scattering-angle dependent alignment parameters or polarization moments of the differential cross section, defined in the stationary-target frame, can then be made using Eqs. (B1)–(B5) above.

APPENDIX C: AVERAGE POLARIZATION MOMENTS

The probe-laser-polarization dependence of the experimental time-of-flight signal (with different times of flight corresponding to different laboratory-frame speeds v_Z) can, in principle, be analyzed using Eq. (3) of the main text to extract the speed-dependent alignment parameters for all possible product laboratory-frame speeds. We prefer a more modest analysis that takes into account our experimental angular resolution. Consequently, we divide the experimental signal into time bins corresponding to certain ranges of laboratory-frame speeds, and hence to certain ranges of scattering angle in the center-of-mass frame. This binning procedure averages over a speed or scattering-angle interval and

thus we determine not the speed and scattering-angle dependent alignment parameters of the above analysis, but the averaged values:

$$\langle f_{kq}^{\mathrm{lab}}(v_{AB})\rangle = \int_{v_{AB}-\Delta v_{AB}}^{v_{AB}+\Delta v_{AB}} f_{kq}^{\mathrm{lab}}(\mathbf{v}_{AB})\mathbf{V}(v_{AB})dv_{AB}, \qquad \text{(C1)}$$

where $2\Delta v_{AB}$ is the speed interval averaged over, and $V(v_{AB})$ is a volume element that depends on the precise nature of the experiment. For a core-extraction experiment in which the core extractor diameter is much smaller than the diameter of the ion packet that impinges on it, $V(v_{AB})=v_{AB}^2$.

We wish to relate the moments in the laboratory frame averaged over a speed range $2\Delta v_{AB}$ to the moments in the stationary-target frame averaged over a corresponding angular range $2\Delta\theta_r$. These stf average moments are defined as

$$\left\langle \frac{1}{\sigma}\frac{d\sigma_{kq}}{d\,\cos\,\theta_r}\right\rangle = \int_{\theta_r-\Delta\theta_r}^{\theta_r+\Delta\theta_r}\frac{1}{\sigma}\left(\frac{d\sigma_{kq}}{d\,\cos\,\theta_r}\right)d\,\cos\,\theta_r. \qquad \text{(C2)}$$

We connect the stf and lab-frame average moments via the relationships of Eqs. (B1)–(B5). Thus, for example,

$$\langle f_{k0}^{\mathrm{lab}}(v_{AB})\rangle = \int_{\theta_r-\Delta\theta_r}^{\theta_r+\Delta\theta_r}\frac{V(v_{AB})}{2v_{AB}^2}\,[1+\beta_{\mathrm{phot}}P_2(\cos\,\theta_u) \times P_2(\cos\,\theta_\epsilon)]\,\frac{1}{\sigma}\left(\frac{d\sigma_{k0}}{d\,\cos\,\theta_r}\right)d\,\cos\,\theta_r, \qquad \text{(C3)}$$

where we have used $d\,\cos\,\theta_r=(v_{AB}/uu_{AB})dv_{AB}$.

This integral presents difficulties unless we can make some simplifying approximations because both v_{AB} and $\cos\,\theta_u$ depend on the scattering angle. We consider two cases: (i) The interval averaged over is small, so that $\cos\,\theta_u$ and v_{AB} vary little with the (small) change in $\cos\,\theta_r$; and (ii) The kinematics of the reaction are such that v_{AB} and $\cos\,\theta_u$ vary little over a wide range of scattering angles (the reaction examined in this paper is such a system for which θ_u varies from 0° to 18° over the full range of scattering angles). In both these cases we can replace $P_2(\cos\,\theta_u)$ by an averaged value, and likewise for v_{AB} and the volume element term (unless they cancel one another). We obtain the result:

$$\langle f_{k0}^{\mathrm{lab}}(v_{AB})\rangle \approx \frac{1}{2}\,[1+\beta_{\mathrm{phot}}\langle P_2(\cos\,\theta_u)\rangle P_2(\cos\,\theta_\epsilon)] \times\left\langle\frac{1}{\sigma}\frac{d\sigma_{k0}}{d\Omega}\right\rangle \qquad \text{(C4)}$$

The connection can thus be made between alignment parameters defined in the stationary-target and laboratory frames that are averaged over certain scattering-angle intervals.

[1] W. R. Simpson, A. J. Orr-Ewing, and R. N. Zare, Chem. Phys. Lett. **212**, 163 (1993).
[2] W. R. Simpson, A. J. Orr-Ewing, T. P. Rakitzis, S. A. Kandel, and R. N. Zare, J. Chem. Phys. **103**, 7299 (1995).
[3] W. R. Simpson, T. P. Rakitzis, S. A. Kandel, A. J. Orr-Ewing, and R. N. Zare, J. Chem. Phys. **103**, 7313 (1995).
[4] W. R. Simpson, Ph.D. thesis, Stanford University (1995).
[5] W. R. Simpson, T. P. Rakitzis, S. A. Kandel, T. Lev-On, and R. N. Zare, J. Phys. Chem. **100**, 7938 (1996).
[6] A. J. Orr-Ewing and R. N. Zare, Annu. Rev. Phys. Chem. **45**, 315 (1994).
[7] Y. Matsumi, K. Tonokura, and M. Kawasaki, J. Chem. Phys. **97**, 1065 (1992).
[8] N. E. Shafer, A. J. Orr-Ewing, W. R. Simpson, H. Xu, and R. N. Zare, Chem. Phys. Lett. **212**, 155 (1993).
[9] F. J. Aoiz, M. Brouard, P. A. Enriquez, and R. Sayos, J. Chem. Soc. Faraday Trans. **89**, 1427 (1993).
[10] H. L. Kim, M. A. Wickramaaratchi, X. N. Zheng, and G. E. Hall, J. Chem. Phys. **101**, 2033 (1994).
[11] N. E. Shafer, H. Xu, R. P. Tuckett, M. Springer, and R. N. Zare, J. Phys. Chem. **98**, 3369 (1994).
[12] H. Xu, N. E. Shafer-Ray, F. Merkt, D. J. Hughes, M. Springer, R. P. Tuckett, and R. N. Zare, J. Chem. Phys. **103**, 5157 (1995).
[13] R. N. Dixon, J. Chem. Phys. **85**, 1866 (1986).
[14] M. Brouard, S. P. Duxon, P. A. Enriquez, and J. P. Simons, J. Chem. Phys. **97**, 7414 (1993).
[15] M. Brouard, H. M. Lambert, C. L. Russell, J. Short, and J. P. Simons, Faraday Disc. Chem. Soc. **102**, (1995); M. Brouard, H. M. Lambert, J. Short, and J. P. Simons, J. Phys. Chem. **99**, 13 571 (1995); M. Brouard, S. P. Duxon, and J. P. Simons, Isr. J. Chem. **34**, 67 (1994); M. Brouard, S. P. Duxon, P. A. Enriquez, and J. P. Simons, J. Chem. Soc. Faraday Trans. **89**, 1435 (1993).
[16] A. J. Alexander, M. Brouard, S. P. Rayner, and J. P. Simons, Chem. Phys. **207**, 215 (1996).
[17] M. Brouard, H. M. Lambert, S. P. Rayner, and J. P. Simons, Mol. Phys. **89** (1996).
[18] M. L. Coston, G. Hancock, A. J. Orr-Ewing, and D. Summerfield, J. Chem. Phys. **100**, 2754 (1994).
[19] T. L. D. Collins, A. J. McCaffery, J. P. Richardson, R. J. Wilson, and M. J. Wynn, J. Chem. Phys. **102**, 4419 (1995); K. L. Reid and A. J. McCaffery, *ibid.* **96**, 5789 (1992).
[20] H. Ni, J. M. Serafin, and J. J. Valentini, J. Chem. Phys. **104**, 2259 (1996), *ibid.*, Chem. Phys. Lett. **244**, 207 (1995).
[21] N. E. Shafer-Ray, A. J. Orr-Ewing, and R. N. Zare, J. Phys. Chem. **99**, 7591 (1995).
[22] W. W. Wiley and I. H. McLaren, Rev. Sci. Intrumen. **26**, 1150 (1955).
[23] A. C. Kummel, G. O. Sitz, and R. N. Zare, J. Chem. Phys. **85**, 6874 (1986).
[24] A. J. Orr-Ewing, W. R. Simpson, T. P. Rakitzis, and R. N. Zare, Isr. J. Chem. **34**, 95 (1994).
[25] R. N. Zare, *Angular Momentum* (Wiley, New York, 1988).
[26] X. Wang, M. Ben-Nun, and R. D. Levine, Chem. Phys. **197**, 1 (1995).
[27] F. J. Aoiz and L. Bañares, Chem. Phys. Lett. **247**, 232 (1995).
[28] D. E. Manolopoulos (private communication); J. F. Castillo, D. E. Manolopoulos, K. Stark, and H. J. Werner, J. Chem. Phys. **104**, 6531 (1996).